Moving boundary and time-dependent effects on mass transfer from a spherical droplet evaporating in gaseous environment

Simona Tonini* and Gianpietro E. Cossali

[1] *University of Bergamo*
Viale Marconi 2, Dalmine (BG), Italy

**Corresponding author: simona.tonini@unibg.it*

Abstract

Analytic modelling of drop evaporation is often approached under quasi-steady approximation, disregarding the inherent unsteadiness of such phenomenon and the fact that drop radius shrinking due to evaporation settles a moving boundary problem. Such assumption yields simple and very useful analytical solutions of the species conservation equations. However it is known that, after the sudden immersion of a drop in a gaseous environment, a relaxation time is needed to reach quasi-steadiness and the evaporation rate during this period is expected to be much higher than that under steady conditions. The present work is aimed to define the analytical problem of evaporation in a gaseous environment relaxing the above mentioned approximation. The spherically symmetric, time-dependent species conservation equation for vapour transport in a gaseous environment is derived in non-dimensional form accounting for moving boundaries. Numerical solution allows to evaluate the relaxation time as a function of the Spalding mass transfer number and to quantify the evaporated mass during this time lapse.

Keywords: Drop evaporation, moving boundaries, unsteady evaporation.

1. Introduction

The process of liquid drop evaporation into gaseous environment has been the subject of extensive research since decades, due to the complexity of the phenomena involved and to its inherent importance in a huge variety of industrial applications [1]. An extensive literature on the modelling of drop evaporation is available and the need of implementation into CFD codes for reliable dispersed flow predictions led to the development of simplified CPU efficient models.

The first evaporation model was proposed by Maxwell back in 1878 [2], who assumed that evaporation is mainly guided by the vapour species diffusion within the gas phase. Various models have been successively developed accounting for the bulk motion of the vapour and gas mixture surrounding the particle (Stefan flow) [3], convective effect [4], liquid composition [5,6] and high pressure effect [7].

Extensive investigation has been done on the modelling of mass and thermal phenomena occurring within the liquid phase in an evaporating drop. In most conventional CFD codes for spray applications the drop heating is modelled assuming infinite liquid thermal conductivity, thus neglecting temperature gradient inside the drop [8], although the available experimental evidence [9,10] contradicts this assumption. This issue has been addressed introducing a finite effective thermal conductivity that also accounts for liquid recirculation inside the drop [1,8]. All the analytical evaporation models for CFD codes are based on the assumption that the evaporation rate is small enough to neglect the moving boundary effect due to radius shrinking. This hypothesis has been removed by Sazhin et al. in [11,12], who included the effect of a moving boundary to solve the heat conduction equation in the liquid phase. Their results evidenced that the effect of drop shrinking on liquid temperature predictions cannot be ignored and the evaporation times are longer compared to the conventional approach.

When modelling the vapour and energy transfer through the gas phase many simplifications are usually assumed, like constancy of the gaseous mixture properties, ideal gas behaviour, spherical symmetry and quasi-steadiness [1]. The last assumption is based on the observation that the time scales of the energy and species transport within the liquid phase are much larger than the corresponding ones into the gas phase. Therefore, the commonly used steady-state drop evaporation models do not account by the fact that when the drop is suddenly immersed in a gas there is a period of relaxation before the quasi-steady state is reached. The aim of this investigation is to quantify the effect of unsteady conditions on drop evaporation, focusing on the vapour transport within the gas phase.

2. Model equations

The time dependent species conservation equations in a binary mixture are:

$$\rho \frac{\partial \chi^{(p)}}{\partial t} = -\nabla_j n_j^{(p)} \quad p = 0,1 \tag{1}$$

where p=1 stands for the evaporating species. The radial component of the species flux from an evaporating single component drop can be written, accounting for the spherical symmetry, as:

$$n_r^{(p)} = \rho U \chi^{(p)} - \rho D_{1,0} \frac{\partial \chi^{(p)}}{\partial r} \quad p = 0,1 \tag{2}$$

where U is the radial component of the mixture mass averaged velocity [13]. The model assumes a constant reference value for

*Footnotes may appear on the first page only to indicate research grant, sponsoring agency, etc. These should not be numbered but referred to by symbols, e.g. *,+. The footnote text may be produced in a small font.

the gaseous mixture density and for the diffusion coefficient. The continuity equation, that can be obtained summing equations (2), can be written as $\nabla_j \rho U_j=0$ and yields the following general solution:

$$\rho U = \frac{m_T(t)}{4\pi r^2} \tag{3}$$

Where $m_T(t)=m^{(0)}(t)+m^{(1)}(t)$ is the total mass flow rate. Equations (1) and (3), accounting for equation (2), are linearly dependent, then one of them can be eliminated retaining the independent set:

$$\rho\frac{\partial \chi^{(1)}}{\partial t} = -\frac{m_T(t)}{4\pi r^2}\frac{\partial \chi^{(1)}}{\partial r} + \rho D_{1,0}\left(\frac{\partial^2 \chi^{(1)}}{\partial r^2} + \frac{2}{r}\frac{\partial \chi^{(1)}}{\partial r}\right) \tag{4a}$$

$$\rho U = \frac{m_T(t)}{4\pi r^2} \tag{4b}$$

2.1. Initial and boundary conditions

Since the aim of this investigation is to evaluate the effect of unsteady evaporation on a drop suddenly injected into a hot gas, the initial conditions for the vapour mass fraction distribution will be considered uniform and equal to the value at infinite:

$$\chi^{(1)}(r,0) = \chi_\infty^{(1)} \qquad r \in [R_0, \infty] \tag{5}$$

Moreover, when a single component drop evaporates in a foreign non isothermal gas, the drop surface temperature, after an initial heat up process, often reaches a plateau and remains constant for almost all the remaining drop life time, with the exception of the very short last stage [1]. Therefore, for a quite long part of the drop evaporation time the vapour mass fraction at drop surface can be considered constant and the spatial B.C. that will be considered here are then of Dirichlet type:

$$\chi^{(1)}(r=R_0,t) = \chi_s^{(1)}; \quad \chi^{(1)}(r=\infty,t) = \chi_\infty^{(1)} \tag{6}$$

Defining the non-dimensional vapour mass fraction as:

$$X = \frac{\chi^{(1)} - \chi_\infty^{(1)}}{\chi_s^{(1)} - \chi_\infty^{(1)}} \tag{7}$$

The differential problem becomes:

$$\rho\frac{\partial X}{\partial t} = \left(\frac{2\rho D_{1,0}}{r} - \frac{m_T(t)}{4\pi r^2}\right)\frac{\partial X}{\partial r} + \rho D_{1,0}\frac{\partial^2 X}{\partial r^2}$$
$$X(R_0,t)=1;\ X(\infty,t)=0;\ \ X(r,0)=0 \tag{8}$$

During the process the drop radius shrinks and the problem (8) is then a moving boundary (Stefan) problem.

The function $m_T(t)$ can be related to the drop radius shrinking by recalling the interface (jump) species balance at the drop surface, that can be written as [13, page 451]:

$$\rho_L^{(p)}\left[U_L^{(p)}(R_0) - V_s\right] - \rho^{(p)}\left[U^{(p)}(R_0) - V_s\right] = 0 \tag{9}$$

where the pedex L is used to indicate the values inside the liquid phase; $\rho_L^{(p)} = \rho_L \chi_L^{(p)}$, ρ_L is the liquid density and $\chi_L^{(p)}$ is the mass fraction of the species p inside the liquid.

The condition that the gas species does not diffuse into the liquid allows to say that $\chi_L^{(0)} = 0$ and $U_L^{(0)} = 0$. Moreover, since the liquid inside the drop is considered still $U_L^{(p)} = 0$ and the interface velocity V_s is related to the radius shrinking by $V_s = \dot{R}_0$, equations (9) yield:

$$U^{(0)}(R_0) = V_s; \quad \left(\rho^{(1)} - \rho_L\right)\dot{R}_0 = \rho^{(1)}U^{(1)}(R_0) \tag{10}$$

and

$$m_T(t) = 4\pi R_0^2 U(R_0) = 4\pi R_0^2\left(\rho - \rho_L\right)\dot{R}_0 \tag{11}$$

2.2. Fixed boundary problem

Consider the following coordinates transformation:

$$\zeta = \zeta(r,t) = \frac{R_0(t)}{r} = \frac{R_{0,i}\varphi(t)}{r}; \quad \tau = \tau(r,t) = \frac{tD_{1,0}}{R_0^2} \tag{12}$$

where $\varphi(t) = \dfrac{R_0(t)}{R_{0,i}}$ and $R_{0,i}=R_0(0)$. The vapour mass flow rate can be calculated integrating the vapour flux (2) over the drop surface (i.e. ζ=1), but also from the interface conditions (the second of equations 10), and equating the two forms yields the following equation for the non-dimensional drop radius $\varphi(t)$:

$$\varphi\dot{\varphi} = -\beta B W(\tau) \tag{13}$$

where $\beta = \dfrac{\rho}{\rho_L}$, $B = \left(\dfrac{\chi_s^{(1)} - \chi_\infty^{(1)}}{1-\chi_s^{(1)}}\right)$, $W(\tau) = \left(\dfrac{\partial X}{\partial \zeta}\right)_{\zeta=1}$, and the integration, with the initial condition $\varphi(0)=1$, yields the explicit solution:

$$\varphi(\tau) = \left[1 - 2\beta B\int_0^\tau W(s)ds\right]^{1/2} \tag{14}$$

To find the gradient of X at ζ=1, the problem (8) can be written in non-dimensional form in the new coordinate system (12) where now the boundaries are fixed; using equation (13) and (14):

$$\dot{X} = \left(\frac{\left[(1-\beta)\zeta^4 + \beta\zeta\right]BW(\tau)}{1 - 2\beta B\int_0^\tau W(s)ds}\right)X' + \left(\frac{\zeta^4}{1 - 2\beta B\int_0^\tau W(s)ds}\right)X'' \tag{15}$$
$$X(1,\tau)=1;\ X(\infty,\tau)=0;\ \ X(\zeta,0)=0$$

where $\dot{X} = \left(\dfrac{\partial X}{\partial \tau}\right)_\zeta$ and $X' = \left(\dfrac{\partial X}{\partial \zeta}\right)_\tau$.

2.3. Numerical implementation and test cases

The problem (15) was numerically implemented using a finite difference scheme. To avoid the instability caused by the discontinuity at drop surface (ζ=1) at the initial time τ=0, the initial conditions where implemented as follows:

$$X(\zeta,0) = f(\zeta) = e^{\frac{R_0}{\delta}\left(\frac{1-\zeta}{\zeta}\right)} \tag{16}$$

where δ can be chosen sufficiently small to approximate the real initial condition to an acceptable extent. A parametric analysis was performed on the dependence of the numerical results on the value of δ/R_0, showing that a safe choice is δ/R_0 smaller than

0.001. Grid independence tests were performed to choose the appropriate cell dimensions.

In the following investigation the values of β were chosen to cover realistic ranges of density ratios: from β=0.001 (water drop in air at atmospheric pressure) to β=0.04 (hydrocarbon drop evaporating under Diesel engine conditions). The vapour mass fraction at infinite was set to zero ($\chi_{\infty}^{(1)}=0$) while its values at drop surface (and consequently the values of *B*) were chosen in a range representing real evaporating conditions.

3. Results and discussion

A sample of the numerical solution of equation (15) at different non-dimensional times is reported in Figure 1 for the case of *B*=0.5 and β=0.04. As expected at the very beginning of the process the gradient of the mass fraction distribution close to the drop surface (ζ=1) is very large, which results in a value of the evaporation rate much larger than that obtained by the quasi-steady approximation.

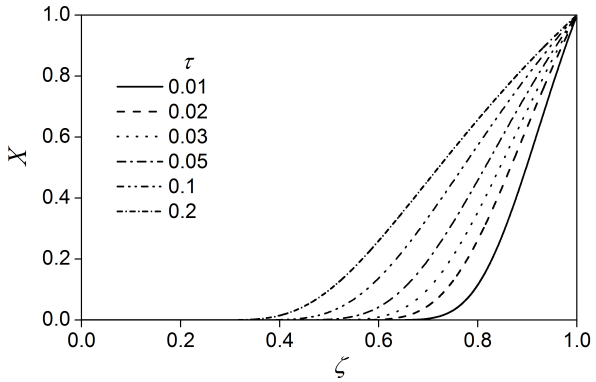

Figure 1. Non-dimensional vapour distribution predicted by the numerical solution of equation (15) at different non-dimensional times; β=0.04 and *B*=0.5.

The drop evaporation rate is the key parameter for all evaporation models; it can be defined as:

$$m_{ev}=-\frac{dM_d(t)}{dt};\qquad M_d(t)=\frac{4}{3}\pi R_0^3\rho_L \tag{17}$$

and using equations (10), (13) and (14) yields:

$$\hat{m}_{ev}=\frac{m_{ev}}{4\pi R_{0,i}\rho D_{10}}=BW(\tau)\left[1-2\beta B\int_0^{\tau}W(s)ds\right]^{1/2} \tag{18}$$

As already mentioned, since the diffusion time scale in the liquid drop is much larger than the corresponding value in the gas, the drop evaporation vapour transport through the gas is usually assumed to be quasi-steady. The most used model in CFD codes is that of [4] that is an extension to convective condition of the Fuchs model [3]. The latter predicts the following form of the evaporation rate:

$$\hat{m}_{ev}^{qs}=\frac{m_{ev}^{qs}}{4\pi R_{0,i}\rho D_{1,0}}=\varphi^{qs}\ln(1+B) \tag{19}$$

that in conjunction with the mass balance (17) yields the following rule (a form of the D^2-law) for the non-dimensional drop radius shrinking:

$$\varphi^{qs}(\tau)=\left[1-2\beta\ln(1+B)\tau\right]^{1/2} \tag{20}$$

Figure 2 shows the values of the non-dimensional radius φ, as function of the non-dimensional time τ, calculated from the numerical solution of the time-dependent problem (equation 14) and from equation (20) for comparison. The graph refers to the case with β=0.04 and *B*=0.5. Due to the large mass fraction gradients close to the drop surface, the initial evaporation rate is higher (up to some orders of magnitude) than that predicted by the quasi-steady approximation and consequently the drop radius decreases faster at the early stage of evaporation, as reported in Figure 2. At later times, the evaporation rates predicted by the moving boundary model and by the quasi-steady one (equations 18 and 19, respectively) become closer, as reported in Figure 3, under the same operating conditions of Figure 2, explaining while the two curves of Figure 2 remain almost parallel.

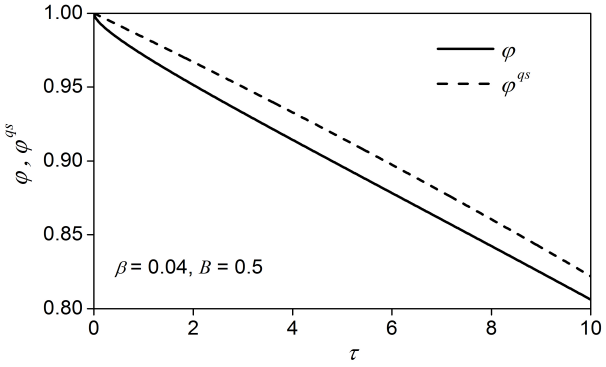

Figure 2. Transient profile of non-dimensional radius predicted by the numerical solution of the time-dependent problem and by the quasi-steady model; β=0.04 and *B*=0.5.

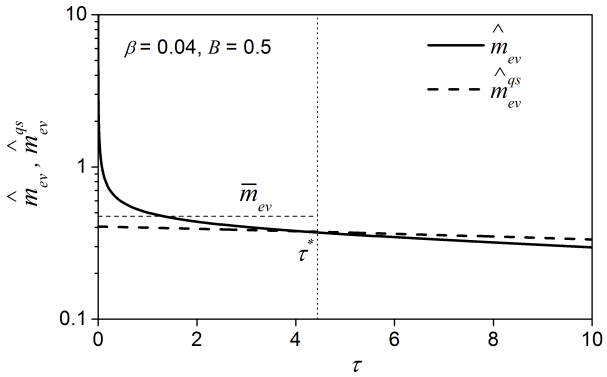

Figure 3. Transient profile of non-dimensional evaporation rate predicted by the numerical solution of the time-dependent problem and by the quasi-steady model; β=0.04 and *B*=0.5.

Figure 3 also shows the characteristic time τ^*, which corresponds to the time when the time derivative of the non-dimensional drop radius predicted by the two models is the same and this is almost coincident (less than 0.1%) to the instant corresponding to the intersection between the two evaporation rate profiles, as reported in Figure 3. This parameter is quite important, since it provides an estimation of the time interval during which the evaporation rate may be much larger than that estimated by the quasi-steady approximation.

A parametrical analysis on the effect of the parameters B and β on the characteristic time τ^* is shown in Figure 4(a), covering a rather wide range of test case applications. The selected values of B ranges from low (B=0.5) up to high (B=10) evaporation rate conditions and the values of β ranges from 0.001 (water drop evaporating at atmospheric conditions) up to 0.04 (Diesel drop in high pressure environment). The results evidence that the characteristic time needed for the two solutions to get closer monotonically decreases as the parameter B increases, suggesting that at lower evaporation rate conditions the effect of accounting for a moving boundary solution becomes more evident and it decreases as β increases.

Figure 4(b) shows the evaporated mass (non-dimensionalised by the drop initial mass) at time τ^*, calculated by the time-dependent and by the quasi-steady solutions, as function of the two parameters B and β. The graph shows that the evaporated mass up to the characteristic time τ^* is higher for the time-dependent solution within the whole range of selected test cases. The evaporated mass at the characteristic time τ^* slightly decreases as the parameter B varies from 0.5 to 10, while it increases up to an order of magnitude increasing β from 0.001 up to 0.04. The relative difference between the two predicted evaporated mass at time τ^* reaches about 6% for the largest selected value of gas/liquid density ratio. This result show that for particular applications, like for example fuel injection under typical Diesel conditions, neglecting the effect of time-dependent evaporation may lead to unneglectable underestimation of the evaporating mass, with an obvious influence on the drop lifetime.

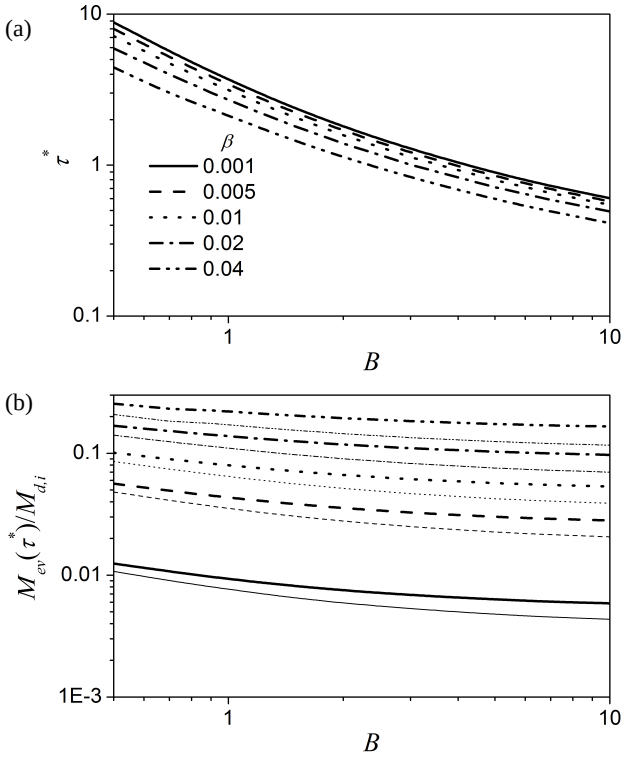

Figure 4. Effect of parameters B and β on (a) the non-dimensional characteristic time τ^*, (b) the evaporated mass at time τ^*, relative to the drop initial mass, predicted by the time-dependent (thick lines) and quasi-steady (thin lines) models.

To mitigate this effect, when using the quasi-steady approach, the evaporation rate during the characteristic period 0-τ^* can be corrected by a multiplying factor defined as follows. The average evaporation rate from 0 to t^* can be calculated as:

$$\overline{m}_{ev} = C\,\overline{m}_{ev}^{qs} \cong C\,m_{ev}^{qs} \tag{21}$$

where $C = \dfrac{M_{ev}}{M_{ev}^{qs}}$ and the last equality comes from the observation that the quasi-steady evaporation rate is practically constant during the characteristic period. The value of $\overline{m}_{ev}$ is reported in Figure 3 for the specific case of β=0.04 and B=0.5.

Therefore a possible approximation of the evaporation rate can be the following:

$$m_{ev} = \begin{cases} C\ m_{ev}^{qs} & \tau < \tau^* \\ m_{ev}^{qs} & \tau \geq \tau^* \end{cases} \tag{22}$$

where the values of C are reported in Figure 5. The correction factor C increases both with B and β, varying from about 1.15 up to 1.4 for the selected range of operating conditions.

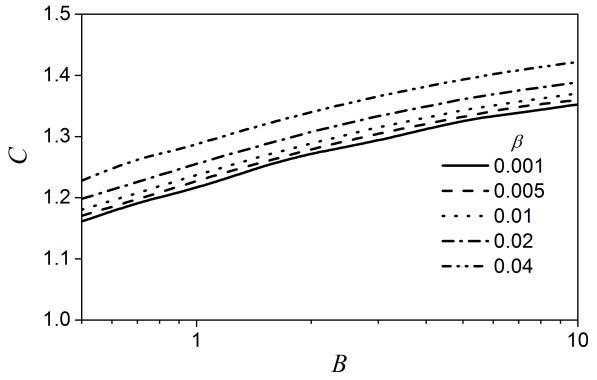

Figure 5. Effect of parameters B and β on the values of the correction factor C in equation (21).

4. Conclusions

The effect of drop shrinking and time-dependent vapour transport was included in the modelling of single-component drop evaporation. The moving boundary problem was transposed into a fixed boundary one through a proper reference system transformation. The model was used to evaluate the evaporation characteristics in a range of operating conditions typical of spray applications.

The time-dependent effects lead to considerable increase of the evaporation rate at the beginning of the process. The relaxation time, needed to reach a quasi-steady condition, was quantified as a function of the Spalding mass transfer number and the gas/liquid density ratio. The increase of evaporated mass during the relaxation time compared to the classical quasi-steady model was evaluated, reaching 6% for the highest gas/liquid density ratio here investigated. A correction factor in the classical quasi-steady evaporation model accounting for the increase of evaporated mass due to time-dependent was proposed.

5. Nomenclature

Roman symbols

B	[-]	Spalding mass transfer number
C	[-]	Correction factor, equation (21)
$D_{1,0}$	[m^2/s]	Diffusion coefficient
M_d	[kg]	Drop mass
M_{ev}	[kg]	Evaporated mass
m_{ev}	[kg/s]	Mass evaporation rate
m_T	[kg/s]	Total mass flow rate
n	[kg/m^{2}s]	Mass flux
r	[m]	Radial coordinate
R_0	[m]	Drop radius
s	[-]	Integration variable, equation (14)
t	[s]	Time
U	[m/s]	Stefan flow velocity
V_s	[m/s]	Interface velocity
X	[-]	Non-dimensional vapour mass fraction
W	[-]	Non-dimensional vapor gradient at surface

Greek symbols

β	[-]	Gas/liquid density ratio
δ	[m]	Characteristic length, equation (16)
χ	[-]	Mass fraction
ρ	[kg/m^3]	Mass density
τ	[-]	Non-dimensional time, $\tau = tD^{(1,0)}/R_0^2$
τ^*	[-]	Characteristic non-dimensional time
φ	[-]	Non-dimensional radius, $\varphi(t) = R_0(t)/R_{0,i}$
ζ	[-]	Non-dimensional radial coordinate, $\zeta = R_0/r$

Subscripts

i	Initial
L	Liquid
qs	Quasi-steady
s	Surface
v	Vapour
∞	Free stream condition

Superscripts

p	Species index
^	Non-dimensional

References

[1] S. Sazhin, Droplets and Sprays, Springer, 2014.
[2] J.C. Maxwell, Diffusion, in: Encyclopaedia Britannica, 9th ed., vol. 7, 1877, p. 214.
[3] N.A. Fuchs, Vaporisation and droplet growth in gaseous media, Pergamon Press, London, 1959.
[4] B. Abramzon, W.A. Sirignano, Droplet vaporization model for spray combustion calculations, Int. J. Heat Mass Transfer 32(9) (1989) 1605-1618.
[5] A.Y. Tong, W.A. Sirignano, Multicomponent transient droplet vaporization with internal circulation: integral equation formulation, Numer. Heat Transfer 10 (1986) 253-278.
[6] Y. Zeng, C.F. Lee, Multicomponent-fuel film-vaporization model for multidimensional computations, J. Propulsion and Power 16 (2000) 964-973.
[7] S.K. Aggarwal, H.C. Mongia, Multicomponent and high-pressure effects on droplet vaporization, J. Eng. Gas Turbines Power 24 (2002) 248-255.
[8] W.A. Sirignano, Fluid Dynamics and Transport of Droplets and Sprays, 2nd ed., Cambridge University Press, 2010.
[9] G. Castanet, M. Lebouché, F. Lemoine, Heat and mass transfer of combusting monodisperse droplets in a linear stream, Int. J. Heat Mass Transfer 48 (2005) 3261–3275.
[10] C. Maqua, G. Castanet, F. Grisch, F. Lemoine, T. Kristyadi, S.S. Sazhin, Monodisperse droplet heating and evaporation: experimental study and modelling, Int. J. Heat Mass Transfer 51 (15–16) (2008) 3932–3945.
[11] S.S. Sazhin, P.A. Krutitskii, I.G. Gusev, M.R. Heikal, Transient heating of an evaporating droplet, Int. J. Heat Mass Transfer 53(13) (2010) 2826-2836.
[12] S.S. Sazhin, P.A. Krutitskii, I.G. Gusev, M.R. Heikal, Transient heating of an evaporating droplet with presumed time evolution of its radius, Int. J. Heat Mass Transfer 54(5) (2011) 1278-1288.
[13] J.C. Slattery, Momentum, Energy and Mass Transfer in Continua, 2nd ed., vol. 482, R. Krieger Publ., New York, 1981.